

Breaking Scaling Relationships in CO₂ Reduction on Copper Alloys with Organic Additives

Yungchieh Lai,[#] Nicholas B. Watkins,[#] Alonso Rosas-Hernández, Arnaud Thevenon, Gavin P. Heim, Lan Zhou, Jonas C. Peters,^{*} John M. Gregoire,^{*} Theodor Agapie^{*}

Division of Chemistry and Chemical Engineering, California Institute of Technology, Pasadena, CA, USA.

[#]These authors contributed equally to this work. ^{*}e-mail: jpeters@caltech.edu; gregoire@caltech.edu; agapie@caltech.edu

Abstract

Boundary conditions for catalyst performance in the conversion of common precursors such as N₂, O₂, H₂O, and CO₂ are governed by linear free energy and scaling relationships. Knowledge of these limits offers an impetus for designing strategies to alter reaction mechanisms to improve performance. Towards a more sustainable carbon economy, understanding the basis of catalytic selectivity for CO₂ conversion to chemical feedstocks/fuels is key. Herein, high-throughput experimentation on 14 bulk copper bimetallic alloys allowed for data-driven identification of a fundamental linear scaling relationship between methane and C₂₊ products that constrains the Faradaic efficiency for C–C coupling. We have furthermore demonstrated that coating the electrodes with a molecular film breaks the scaling relationship to promote C₂₊ product formation.

Introduction

The development of high-performing catalysts for sustainable and economically viable transformations remains a central goal of the chemical industry.¹ Chemical transformations are controlled by thermodynamic and kinetic rate laws that manifest as linear scaling relationships. Such relationships relating structure, activity, and reaction conditions, are established for a range of reactions, including H₂O oxidation and N₂, O₂, CO₂, and H₂O reduction performed on both heterogeneous and homogeneous catalysts.^{1–7} Because they provide theoretical or empirical trends for a particular chemical process, these scaling relationships not only help explain chemical reactivity but also guide the rational design of new and improved catalysts. Determining the underlying connections in chemical processes is particularly desirable toward deconvoluting fundamental selectivity limitations and targeting specific products.^{2,8} CO₂ reduction (CO₂R) on Cu electrodes is one particular example where mechanistic complexity has hindered catalyst optimization and warrants further investigation.⁹

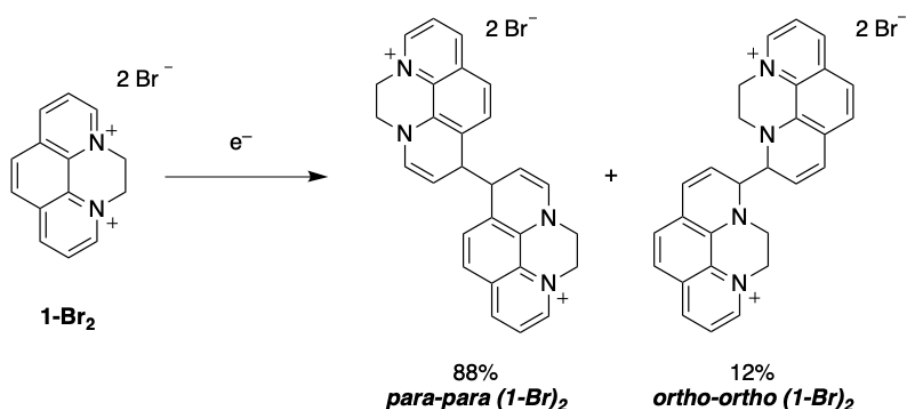
As strategies to transform CO₂ at scale are considered for a more sustainable carbon economy, exploiting the unique ability of Cu to reduce CO₂ to C₂₊ hydrocarbons and oxygenates makes it an attractive catalyst for optimization. The complex pathways towards a myriad of reduced products of CO₂R on Cu stymie efforts for producing carbon-coupled products with high selectivity and has prompted investigation into the mechanism of the transformation.⁹ Systematic trends affecting selectivity have been shown with respect to adsorption energy scaling relationships and pH variation at the electrode surface.^{10–13} Promising strategies for improving CO₂R selectivity for C₂₊ products include changing catalyst morphology^{14–17} and electrolyte composition,^{12,18} employing bimetallic systems and alloys,^{19–21} and adding organic modifiers.^{22–27} However, identifying empirical scaling relationships from the published data is challenging due to substantial variation in catalyst preparation and electrochemical testing conditions across independent studies, highlighting the need for studies that systematically and broadly vary select parameters.

We have developed a high throughput screening system for accelerated catalyst discovery whose improved automation and operation make it particularly well suited for this application.^{28,29} We have identified bulk alloying of Cu as an underdeveloped, though promising strategy for catalyst optimization, with a large parameter space available based on the metal identity and composition.^{30,31} Additionally, organic additives represent an attractive orthogonal parameter of catalyst design. They can impact performance in a manner that has seldom been achieved by tailoring inorganic electrocatalyst composition or morphology alone.³²

Inspired by recent success using molecular films to enhance the selectivity of catalysts for CO₂R,^{27,33–35} herein we describe the generation of a uniquely broad and systematic CO₂R catalyst database by combining a Cu bimetallic alloying strategy with the use of organic additives. Selectivity analysis reveals scaling relationships for the alloys that is broken upon coating with an organic additive, demonstrating a fundamental limitation of CO₂R on Cu and a strategy to overcome it through hybrid inorganic-organic interfaces.

Results and Discussion

To elucidate scaling relationships in CO₂R, experiments were designed to observe a large dynamic range of catalyst properties while mitigating conflation with experiment parameters such as electrolyte composition and mass transport conditions. For the present work, we varied catalyst composition, applied potential, and molecular additive presence. The choice of Cu alloys was guided by our previous discovery that the alloying elements In, Co, Mn, and Zn alter the activity and selectivity of Cu in different ways, although that study was limited to detection of H₂, CH₄, and C₂H₄.²⁹ Studying Cu alloys with each of these elements and with different concentrations that span face-centered cubic (fcc) alloys and intermetallic phases, we sought to obtain a more comprehensive map of the reactivity of Cu-based alloy catalysts and to identify any systematic trends. The molecular additive, N,N'-ethylene-phenanthroline dibromide (**1-Br₂**), was selected based on its ability to enhance Faradaic efficiency (FE) and partial current densities for C₂₊ products upon forming a well-defined film on polycrystalline Cu, primarily composed of a *para,para* isomer of the one-electron reduced and dimerized phenanthroline (Equation 1).³³



Equation 1: The electrochemical reductive coupling of two **1-Br₂** molecules results in a mixture of two products.

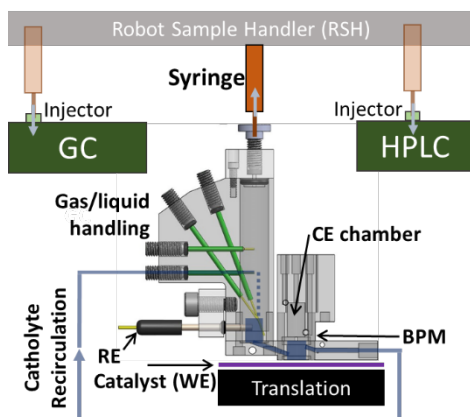


Figure 1: The high throughput catalyst screening system where a select catalyst is positioned under a recirculating electrochemical batch reactor. After electrocatalyst operation, a robot sample handler (RSH) uses a syringe (orange) to extract aliquots from the headspace and then catholyte, with each aliquot injected into the respective analytical instrument (green, syringe positions in translucent orange) for gas or high-pressure liquid chromatography (GC, HPLC). The reference electrode (RE) is placed in the electrolyte inlet to the working electrode (WE) chamber, which is separated from the counter electrode (CE) chamber by a bipolar membrane (BPM).

Catalyst performance with or without the additive was evaluated by chronoamperometry (CA) at a series of up to 6 potentials with subsequent product analysis using the batch reactor flow system illustrated in Fig. 1. This system uses rapid electrolyte flow, as opposed to vigorous CO₂ bubbling, to generate suitable and reproducible mass transport conditions. The rapid concentration of reaction products enhances measurement throughput by enabling shorter electrolysis and faster chromatography compared to traditional methods. Hybrid metal-organic electrodes were prepared via electrodeposition of organic films on the polycrystalline metal electrode from an aqueous 0.1 M KHCO₃ buffered electrolyte containing 0.1 mM **1-Br₂**. In total, experiments with 14 alloy catalysts and pure Cu provide electrochemical and partial current densities for 137 unique combinations of catalyst composition, additive presence, and applied potential, as shown for select Mn-doped catalysts in Figs. 2a-2b and for all catalysts in Figs. S1-S2.

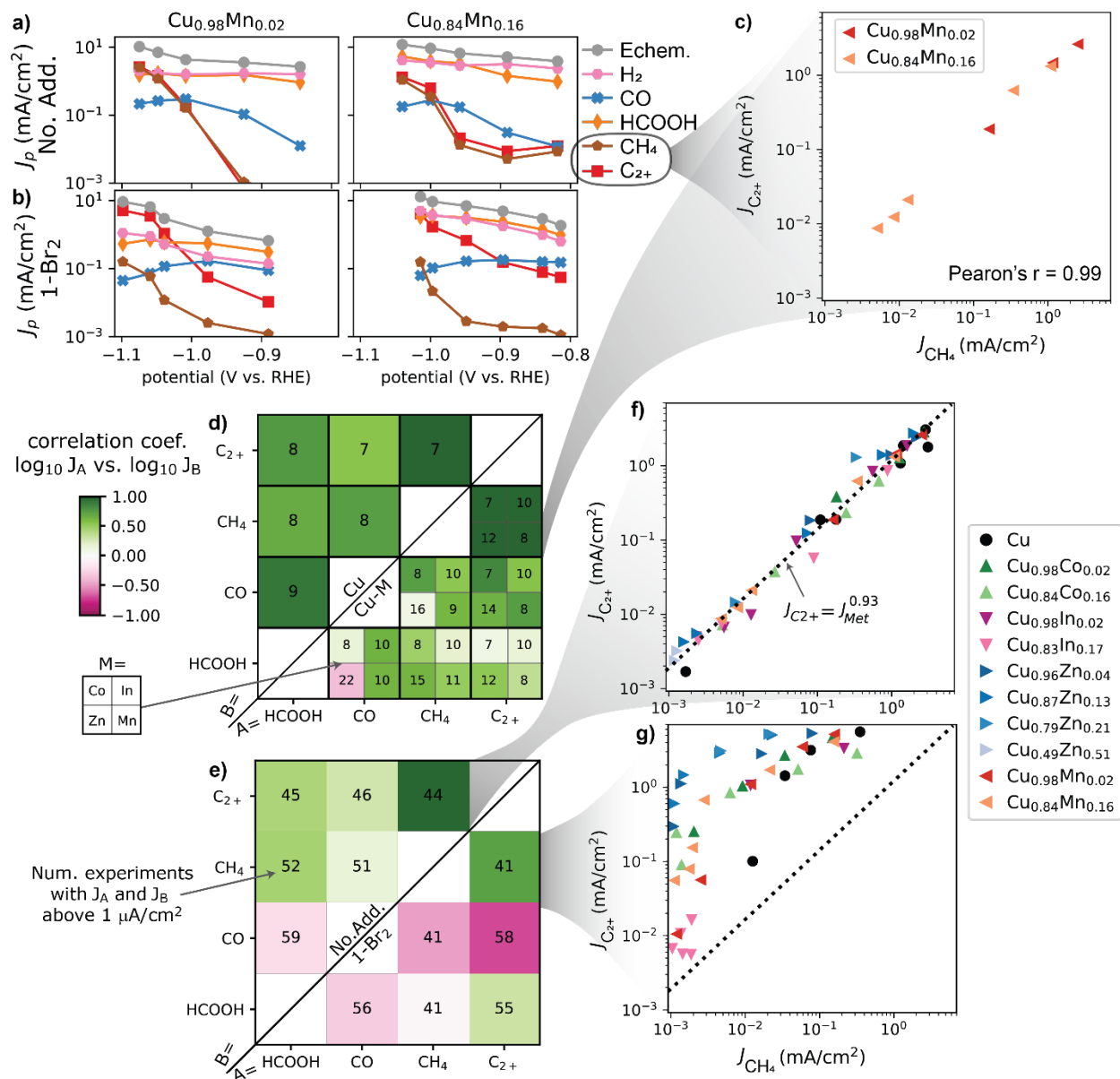


Figure 2: Illustration of acquired data and correlation analysis. The electrochemical and partial current densities are shown for 5 electrolysis experiments with $\text{Cu}_{0.98}\text{Mn}_{0.02}$ and 6 electrolysis experiments with $\text{Cu}_{0.84}\text{Mn}_{0.16}$ catalysts, both a) without additive and b) with 1-Br₂. Select products or product categories were considered for correlation analysis. For A = CH₄ and B = C₂₊, a) contains 8 electrolysis experiments with partial current densities for both A and B above 1 $\mu\text{A cm}^{-2}$. The corresponding 8 points are shown in c) and used to calculate the Pearson correlation coefficient to represent additive-free Cu-Mn alloys. This analysis was applied to all 6 pairwise combinations of the products HCOOH, CO, CH₄, and C₂₊ and repeated for pure Cu and each Cu-M alloy system. The resulting set of correlation coefficients is shown in d). The printed numbers in each cell indicate the number of electrolysis experiments used in the calculation, for example 8 for the A = CH₄, B = C₂₊, M = Mn cell corresponding to the plot in c). This analysis was also applied to electrolysis experiments from all compositions, first with and then without 1-Br₂, to assess the impact of the additive on the 6 pairwise correlation coefficients, as shown in e). For A = CH₄ and B = C₂₊ in e), the data underlying the correlation analysis is shown in f) without additive and in g) with 1-Br₂, where points are colored according to their composition. The data in f) follow the scaling relationship indicated by the dashed line, which is also depicted in g) to show the extent by which the data with 1-Br₂ deviate from this scaling relationship.

Pairwise relationships of the partial current density and the FE for representative products (Fig. S3) highlight the effect of the combined strategy of alloying and organic films. The intrinsic modification of catalyst selectivity can be detected through analysis of the Pearson correlation coefficient of the logarithm of partial current densities. A close-to-unity positive correlation indicates that selectivity between the two products cannot be tuned with the parameters under consideration, which is indicative of a free-energy scaling relationship. A substantially negative correlation indicates a trade-off in selectivity, wherein enhanced formation of one product occurs at the expense of the other, which is indicative of kinetic competition for a shared reaction intermediate.

The large dataset provided here via high throughput experimentation enables study of correlation coefficients and their modification (Fig. 2). Previous work on polycrystalline Cu indicates that the kinetic regimes that govern the CO₂R product distribution differ with applied potential due to modulation of energy landscape as a function of overpotential as well as second-order effects such as CO₂ mass transport and changes to the pH at the catalyst surface.^{36,37} To facilitate observation of how the catalyst itself affects selectivity, we aim to mitigate the influences from the extrinsic effects by limiting the overpotential range (-0.84 to -1.1 V vs RHE) and using rapid electrolyte flow over flat catalyst films with a maximum current density of 15 mA cm⁻², which promotes uniform mass transport and limits pH gradients in the electrochemical reactor. This potential range includes the onset of substantial partial current density for highly reduced products, making alteration of correlation coefficients in this range a prime target for controlling product selectivity with catalyst modification. We first demonstrate Pearson correlation analysis to ascertain the extent by which high correlation coefficients can be lowered via variation in catalyst composition. For example, the box in Fig. 2d with A = CH₄ and B = C₂₊ shows a high correlation coefficient of 0.99 for these products when considering a series of 7 electrolysis experiments with a polycrystalline Cu catalyst in which partial current densities for both CH₄ and C₂₊ products varied from approximately 1 μA cm⁻² to 3 mA cm⁻². The analogous analysis for polycrystalline Cu-M alloys is summarized by the boxes with A = C₂₊ and B = CH₄, where the correlation coefficient was calculated for each alloying element using various combinations of alloy composition and applied potential. The source data and its utilization of correlation analysis are illustrated for the Cu-Mn system in Figs. 2a and 2c.

The total number of electrolysis conditions and range of alloy compositions (x in Cu_{1-x}M_x) are as follows: 7 conditions with M = Co and $x = 0.02$ or 0.16 ; 10 conditions with M = In and $x = 0.02$ or 0.17 ; 16 conditions with M = Zn and $x = 0.04, 0.13, 0.21,$ or 0.51 ; 8 conditions with M = Mn and $x = 0.02$ or 0.16 . Despite the variation in composition and potential within each of these Cu-M systems, each correlation coefficient remains in excess of 0.98, and in total the correlation coefficient for all Cu-M alloys is not meaningfully changed from that observed with pure Cu.

Fig. 2f shows the aggregation of data for Cu and its alloys, demonstrating that a power-law scaling relationship is closely followed over a broad range of composition and applied potential. This striking relationship over three orders of magnitude in partial current densities, strongly suggests that on these bulk alloy catalysts there is a common branching point, or combination of branching points, that consistently partition between and CH₄ and C₂₊ products (Fig. 3a). Preservation of the CH₄ / C₂₊ ratio as observed here represents a newly discovered fundamental limitation for efforts to improve selectivity through bulk bimetallic alloying alone.

A simple rationale for the observed scaling relationship is challenged by the complexity of the mechanism of CO₂R.³⁸ Also, the alloying elements substantially alter other aspects of the product distribution, making

this collection of catalyst electrodes particularly well-suited for inferring intrinsic reactivity trends; the catalyst morphology is kept relatively constant with respect to the compendium of results in the literature.^{9,12,14,15,18–20,22–24,30,39} For example, through study of well-defined Cu surfaces, Hori and others identified that the relative production of CH₄ and C₂H₄ is highly facet-dependent.¹³ The distribution of exposed facets of a polycrystalline fcc-phase metal electrode could be altered via alloying due to changes in growth kinetics and/or relative surface energies upon addition of the alloying element, which would in principle provide a method to break the CH₄-C₂₊ scaling relationship by tuning catalyst composition. The observation that the scaling relationship holds over a broad range of alloy compositions indicates that either no such facet selectivity was obtained, or any surface promoted by the alloy composition is highly selective for 2e⁻ products, such that the impact on CH₄ vs. C₂₊ partial current densities is negligible.

CO₂R to highly-reduced products such as CH₄ and C₂₊ products proceeds via a common *CO intermediate.^{40,41} Methane synthesis is proposed to proceed via a Langmuir-Hinshelwood pathway, where a surface *H couples with *CO to form a *CHO or *COH intermediate that is further hydrogenated towards methane.^{40,42,43} Meanwhile, the production of C₂₊ products occurs via the coupling of two precursor *CO molecules, potentially involving intermediate *CHO adsorbates.^{40,41} Although the specific mechanism/s remain debated and may involve multiple pathways depending on morphology or crystal facet, the observed scaling relationship between CH₄ and C₂₊ indicates that the relative kinetics at the branching point(s), remarkably, remain rigorously locked at the same ratio over the many catalysts and applied potentials tested herein. Breaking this dependence is highly desirable for improved selectivity for C₂₊ products.

The Pearson correlation analysis was extended to the impact of the **1-Br₂** additive (Fig. 2e), where the correlation coefficient for each set of conditions includes the aggregation of all catalyst compositions and potentials. Coating the catalysts using **1-Br₂** lowers the correlation coefficient for CH₄ and C₂₊ from 0.99 to 0.74, a striking alteration whose implication is that, within the range of catalyst compositions considered in the present work, tuning the selectivity between CH₄ and C₂₊ is only achieved in the presence of the additive, underscoring the importance of multi-modal catalyst development.⁴⁴

The basis by which the additive disrupts the linear relationship between CH₄ / C₂₊ (Fig. 2f) by increasing C₂₊ production and suppressing CH₄ formation (Fig 2g) is of particular interest. Fig. 3a illustrates the portion of the CO₂R reaction network wherein branching ratios dictate whether the common CO* intermediate results in the generation of CO, CH₄ or C₂₊ products. Fig. 3b highlights how catalyst modification with the organic additive moves product distribution almost completely away from CH₄, to the CO-C₂₊ vector of the graph. While accessing the CO-rich portion of the graph is commonplace in CO₂R electrocatalysis, the C₂₊-rich portion of the graph is only accessed in the presence of **1-Br₂**.⁹ The maximal selectivity was obtained with a Cu_{0.85}Zn_{0.15} catalyst where 96% of the CO* intermediate was reduced to carbon-coupled products.

The breaking of the scaling relationship in the presence of **1-Br₂** cannot be explained by morphological changes, as no nanostructuring was observed (Figs. S5-S6), therefore suggesting that the molecular additive improves selectivity via changes in the microkinetic pathway/s in this system. The organic additive may affect CH₄ - C₂₊ branching point(s) by i) alleviating a rate limitation of the formation of the bound *CHO/*COH intermediate and lowering the barrier towards C-C coupling or ii) promoting dimerization of the bound *CO relative to hydrogenation toward CH₄. In either case, kinetic competition for the *CO would be enhanced in the presence of the additive, which is consistent with the observation of a large

and negative Pearson correlation between C_{2+} and CO (Fig. 2e). We additionally note that neither of these explanations for the mechanism underlying the scaling law disruption has implications for the selectivity within the set of C_{2+} products. As shown in Fig. S4, additional scaling relationships among these products are observed both in the absence and in the presence of the molecular additive, motivating future tuning of the catalyst system to tackle other branching points in the reaction network for enhanced control over product selectivity.

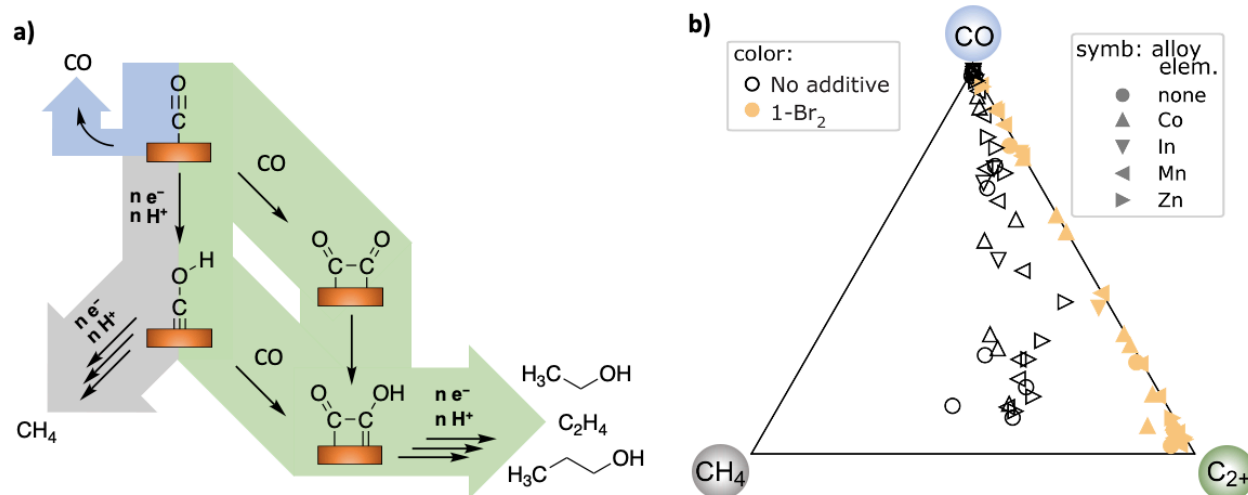


Figure 3: a) Possible reaction mechanisms, where pathways are highlighted with respect to their products in Fig. 3b. There are two branching points between CH_4 and C_{2+} products that could be responsible for the relationship observed in Fig. 2. The strong relationship between the grey and green pathways is broken with the addition of molecular additives, implying a potential change in mechanism. b) Summary of molar selectivity for reduction of the CO^* intermediate. Measured partial current densities for CO, CH_4 and C_{2+} products are converted to molar flux of CO^* required to produce the respective products, whose normalization provides the ternary composition for inclusion in this figure. Each electrolysis experiment produces 1 data point that indicates the catalyst's selectivity with respect to the three reaction pathways highlighted in part a) that start from the common CO^* intermediate.

Conclusion

High throughput screening of the CO_2R activity and selectivity of Cu alloys with Co, In, Mn, and Zn revealed the propensity of organic additive **1- Br_2** to enable development of hybrid electrocatalysts that can reduce CO_2 to high order products with improved activity and selectivity. The large data set led to the observation of a CH_4 - C_{2+} scaling relationship that demonstrates a particularly robust link between these products over a large range of conditions. The CH_4 - C_{2+} relationship represents an intrinsic limitation of selectivity tuning through alloying. However, it can be disrupted to favor C_{2+} products by the presence of the organic additive, highlighting the potential of hybrid organic-inorganic catalysts to tune branching ratios in the CO_2R reaction network. These observations highlight the importance of data-driven identification of relationships that provide mechanistic insights to guide study of complex reactions and catalyst development. Disentangling the possible explanations of the combined mechanistic influence of the additive and alloying elements will require substantial further investigation that will be guided by the observed data relationships elucidated in this study.

Acknowledgment

This material is based on work performed by the Liquid Sunlight Alliance, which is supported by the U.S. Department of Energy, Office of Science, Office of Basic Energy Sciences, Fuels from Sunlight Hub under Award Number DE-SC0021266. A.T. acknowledges Marie Skłodowska-Curie Fellowship H2020-MSCA-IF-2017 (793471). J.C.P. also acknowledges general support from the Resnick Sustainability Institute at Caltech.

Data and materials availability: All material preparation and characterization, synthetic and electrochemical procedures, and raw data is available within the supplementary materials.

References

- (1) Seh, Z. W.; Kibsgaard, J.; Dickens, C. F.; Chorkendorff, I.; Nørskov, J. K.; Jaramillo, T. F. Combining Theory and Experiment in Electrocatalysis: Insights into Materials Design. *Science* **2017**, *355* (6321), eaad4998. <https://doi.org/10.1126/science.aad4998>.
- (2) Pérez-Ramírez, J.; López, N. Strategies to Break Linear Scaling Relationships. *Nat. Catal.* **2019**, *2* (11), 971–976. <https://doi.org/10.1038/s41929-019-0376-6>.
- (3) Greeley, J. Theoretical Heterogeneous Catalysis: Scaling Relationships and Computational Catalyst Design. *Annu. Rev. Chem. Biomol. Eng.* **2016**, *7* (1), 605–635. <https://doi.org/10.1146/annurev-chembioeng-080615-034413>.
- (4) Liu, X.; Xiao, J.; Peng, H.; Hong, X.; Chan, K.; Nørskov, J. K. Understanding Trends in Electrochemical Carbon Dioxide Reduction Rates. *Nat. Commun.* **2017**, *8* (1), 15438. <https://doi.org/10.1038/ncomms15438>.
- (5) Waldie, K. M.; Ostericher, A. L.; Reineke, M. H.; Sasayama, A. F.; Kubiak, C. P. Hydricity of Transition-Metal Hydrides: Thermodynamic Considerations for CO₂ Reduction. *ACS Catal.* **2018**, *8* (2), 1313–1324. <https://doi.org/10.1021/acscatal.7b03396>.
- (6) Ostericher, A. L.; Waldie, K. M.; Kubiak, C. P. Utilization of Thermodynamic Scaling Relationships in Hydricity To Develop Nickel Hydrogen Evolution Reaction Electrocatalysts with Weak Acids and Low Overpotentials. *ACS Catal.* **2018**, *8* (10), 9596–9603. <https://doi.org/10.1021/acscatal.8b02922>.
- (7) Martin, D. J.; Wise, C. F.; Pegis, M. L.; Mayer, J. M. Developing Scaling Relationships for Molecular Electrocatalysis through Studies of Fe-Porphyrin-Catalyzed O₂ Reduction. *Acc. Chem. Res.* **2020**, *53* (5), 1056–1065. <https://doi.org/10.1021/acs.accounts.0c00044>.
- (8) Vojvodic, A.; Nørskov, J. K. New Design Paradigm for Heterogeneous Catalysts. *Natl. Sci. Rev.* **2015**, *2* (2), 140–143. <https://doi.org/10.1093/nsr/nwv023>.
- (9) Nitopi, S.; Bertheussen, E.; Scott, S. B.; Liu, X.; Engstfeld, A. K.; Horch, S.; Seger, B.; Stephens, I. E. L.; Chan, K.; Hahn, C.; Nørskov, J. K.; Jaramillo, T. F.; Chorkendorff, I. Progress and Perspectives of Electrochemical CO₂ Reduction on Copper in Aqueous Electrolyte. *Chem. Rev.* **2019**, *119* (12), 7610–7672. <https://doi.org/10.1021/acs.chemrev.8b00705>.
- (10) Peterson, A. A.; Nørskov, J. K. Activity Descriptors for CO₂ Electroreduction to Methane on Transition-Metal Catalysts. *J. Phys. Chem. Lett.* **2012**, *3* (2), 251–258. <https://doi.org/10.1021/jz201461p>.
- (11) Liu, X.; Schlexer, P.; Xiao, J.; Ji, Y.; Wang, L.; Sandberg, R. B.; Tang, M.; Brown, K. S.; Peng, H.; Ringe, S.; Hahn, C.; Jaramillo, T. F.; Nørskov, J. K.; Chan, K. pH Effects on the Electrochemical Reduction of CO(2) towards C₂ Products on Stepped Copper. *Nat. Commun.* **2019**, *10* (1), 32. <https://doi.org/10.1038/s41467-018-07970-9>.
- (12) Resasco, J.; Chen, L. D.; Clark, E.; Tsai, C.; Hahn, C.; Jaramillo, T. F.; Chan, K.; Bell, A. T. Promoter Effects of Alkali Metal Cations on the Electrochemical Reduction of Carbon Dioxide. *J. Am. Chem. Soc.* **2017**, *139* (32), 11277–11287. <https://doi.org/10.1021/jacs.7b06765>.
- (13) Hori, Y.; Takahashi, I.; Koga, O.; Hoshi, N. Electrochemical Reduction of Carbon Dioxide at Various Series of Copper Single Crystal Electrodes. *J. Mol. Catal. Chem.* **2003**, *199* (1), 39–47. [https://doi.org/10.1016/S1381-1169\(03\)00016-5](https://doi.org/10.1016/S1381-1169(03)00016-5).
- (14) Jeon, H. S.; Kunze, S.; Scholten, F.; Roldan Cuenya, B. Prism-Shaped Cu Nanocatalysts for Electrochemical CO₂ Reduction to Ethylene. *ACS Catal.* **2018**, *8* (1), 531–535. <https://doi.org/10.1021/acscatal.7b02959>.
- (15) Hahn, C.; Hatsukade, T.; Kim, Y.-G.; Vailionis, A.; Baricuatro, J. H.; Higgins, D. C.; Nitopi, S. A.; Soriaga, M. P.; Jaramillo, T. F. Engineering Cu Surfaces for the Electrocatalytic Conversion of CO₂ :

- Controlling Selectivity toward Oxygenates and Hydrocarbons. *Proc. Natl. Acad. Sci.* **2017**, *114* (23), 5918–5923. <https://doi.org/10.1073/pnas.1618935114>.
- (16) Zhang, B.; Zhang, J.; Hua, M.; Wan, Q.; Su, Z.; Tan, X.; Liu, L.; Zhang, F.; Chen, G.; Tan, D.; Cheng, X.; Han, B.; Zheng, L.; Mo, G. Highly Electrocatalytic Ethylene Production from CO₂ on Nanodeficient Cu Nanosheets. *J. Am. Chem. Soc.* **2020**, *142* (31), 13606–13613. <https://doi.org/10.1021/jacs.0c06420>.
- (17) Wang, Y.; Wang, Z.; Dinh, C.-T.; Li, J.; Ozden, A.; Golam Kibria, M.; Seifitokaldani, A.; Tan, C.-S.; Gabardo, C. M.; Luo, M.; Zhou, H.; Li, F.; Lum, Y.; McCallum, C.; Xu, Y.; Liu, M.; Proppe, A.; Johnston, A.; Todorovic, P.; Zhuang, T.-T.; Sinton, D.; Kelley, S. O.; Sargent, E. H. Catalyst Synthesis under CO₂ Electroreduction Favours Faceting and Promotes Renewable Fuels Electrosynthesis. *Nat. Catal.* **2020**, *3* (2), 98–106. <https://doi.org/10.1038/s41929-019-0397-1>.
- (18) Singh, M. R.; Kwon, Y.; Lum, Y.; Ager, J. W.; Bell, A. T. Hydrolysis of Electrolyte Cations Enhances the Electrochemical Reduction of CO₂ over Ag and Cu. *J. Am. Chem. Soc.* **2016**, *138* (39), 13006–13012. <https://doi.org/10.1021/jacs.6b07612>.
- (19) Lum, Y.; Ager, J. W. Sequential Catalysis Controls Selectivity in Electrochemical CO₂ Reduction on Cu. *Energy Environ. Sci.* **2018**, *11* (10), 2935–2944. <https://doi.org/10.1039/C8EE01501E>.
- (20) Morales-Guio, C. G.; Cave, E. R.; Nitopi, S. A.; Feaster, J. T.; Wang, L.; Kuhl, K. P.; Jackson, A.; Johnson, N. C.; Abram, D. N.; Hatsukade, T.; Hahn, C.; Jaramillo, T. F. Improved CO₂ Reduction Activity towards C₂+ Alcohols on a Tandem Gold on Copper Electrocatalyst. *Nat. Catal.* **2018**, *1* (10), 764–771. <https://doi.org/10.1038/s41929-018-0139-9>.
- (21) Zhong, M.; Tran, K.; Min, Y.; Wang, C.; Wang, Z.; Dinh, C.-T.; De Luna, P.; Yu, Z.; Rasouli, A. S.; Brodersen, P.; Sun, S.; Voznyy, O.; Tan, C.-S.; Askerka, M.; Che, F.; Liu, M.; Seifitokaldani, A.; Pang, Y.; Lo, S.-C.; Ip, A.; Ulissi, Z.; Sargent, E. H. Accelerated Discovery of CO₂ Electrocatalysts Using Active Machine Learning. *Nature* **2020**, *581* (7807), 178–183. <https://doi.org/10.1038/s41586-020-2242-8>.
- (22) Wang, J.; Cheng, T.; Fenwick, A. Q.; Baroud, T. N.; Rosas-Hernández, A.; Ko, J. H.; Gan, Q.; Goddard III, W. A.; Grubbs, R. H. Selective CO₂ Electrochemical Reduction Enabled by a Tricomponent Copolymer Modifier on a Copper Surface. *J. Am. Chem. Soc.* **2021**, *143* (7), 2857–2865. <https://doi.org/10.1021/jacs.0c12478>.
- (23) Wei, X.; Yin, Z.; Lyu, K.; Li, Z.; Gong, J.; Wang, G.; Xiao, L.; Lu, J.; Zhuang, L. Highly Selective Reduction of CO₂ to C₂+ Hydrocarbons at Copper/Polyaniline Interfaces. *ACS Catal.* **2020**, *10* (7), 4103–4111. <https://doi.org/10.1021/acscatal.0c00049>.
- (24) Chen, X.; Chen, J.; Alghoraibi, N. M.; Henckel, D. A.; Zhang, R.; Nwabara, U. O.; Madsen, K. E.; Kenis, P. J. A.; Zimmerman, S. C.; Gewirth, A. A. Electrochemical CO₂ -to-Ethylene Conversion on Polyamine-Incorporated Cu Electrodes. *Nat. Catal.* **2021**, *4* (1), 20–27. <https://doi.org/10.1038/s41929-020-00547-0>.
- (25) Buckley, A. K.; Lee, M.; Cheng, T.; Kazantsev, R. V.; Larson, D. M.; Goddard III, W. A.; Toste, F. D.; Toma, F. M. Electrocatalysis at Organic–Metal Interfaces: Identification of Structure–Reactivity Relationships for CO₂ Reduction at Modified Cu Surfaces. *J. Am. Chem. Soc.* **2019**, *141* (18), 7355–7364. <https://doi.org/10.1021/jacs.8b13655>.
- (26) Banerjee, S.; Han, X.; Thoi, V. S. Modulating the Electrode–Electrolyte Interface with Cationic Surfactants in Carbon Dioxide Reduction. *ACS Catal.* **2019**, *9* (6), 5631–5637. <https://doi.org/10.1021/acscatal.9b00449>.
- (27) Han, Z.; Kortlever, R.; Chen, H.-Y.; Peters, J. C.; Agapie, T. CO₂ Reduction Selective for C₂+ Products on Polycrystalline Copper with N-Substituted Pyridinium Additives. *ACS Cent. Sci.* **2017**, *3* (8), 853–859. <https://doi.org/10.1021/acscentsci.7b00180>.

- (28) Jones, R. J. R.; Wang, Y.; Lai, Y.; Shinde, A.; Gregoire, J. M. Reactor Design and Integration with Product Detection to Accelerate Screening of Electrocatalysts for Carbon Dioxide Reduction. *Rev. Sci. Instrum.* **2018**, *89* (12), 124102. <https://doi.org/10.1063/1.5049704>.
- (29) Lai, Y.; Jones, R. J. R.; Wang, Y.; Zhou, L.; Richter, M. H.; Gregoire, J. The Sensitivity of Cu for Electrochemical Carbon Dioxide Reduction to Hydrocarbons as Revealed by High Throughput Experiments. *J. Mater. Chem. A* **2019**, *7* (47), 26785–26790. <https://doi.org/10.1039/C9TA10111J>.
- (30) Gao, D.; Arán-Ais, R. M.; Jeon, H. S.; Roldan Cuenya, B. Rational Catalyst and Electrolyte Design for CO₂ Electroreduction towards Multicarbon Products. *Nat. Catal.* **2019**, *2* (3), 198–210. <https://doi.org/10.1038/s41929-019-0235-5>.
- (31) He, J.; Dettelbach, K. E.; Salvatore, D. A.; Li, T.; Berlinguette, C. P. High-Throughput Synthesis of Mixed-Metal Electrocatalysts for CO₂ Reduction. *Angew. Chem. Int. Ed.* **2017**, *56* (22), 6068–6072. <https://doi.org/10.1002/anie.201612038>.
- (32) Nam, D.-H.; De Luna, P.; Rosas-Hernández, A.; Thevenon, A.; Li, F.; Agapie, T.; Peters, J. C.; Shekhah, O.; Eddaoudi, M.; Sargent, E. H. Molecular Enhancement of Heterogeneous CO₂ Reduction. *Nat. Mater.* **2020**, *19* (3), 266–276. <https://doi.org/10.1038/s41563-020-0610-2>.
- (33) Thevenon, A.; Rosas-Hernández, A.; Peters, J. C.; Agapie, T. In-Situ Nanostructuring and Stabilization of Polycrystalline Copper by an Organic Salt Additive Promotes Electrocatalytic CO₂ Reduction to Ethylene. *Angew. Chem. Int. Ed.* **2019**, *58* (47), 16952–16958. <https://doi.org/10.1002/anie.201907935>.
- (34) Li, F.; Thevenon, A.; Rosas-Hernández, A.; Wang, Z.; Li, Y.; Gabardo, C. M.; Ozden, A.; Dinh, C. T.; Li, J.; Wang, Y.; Edwards, J. P.; Xu, Y.; McCallum, C.; Tao, L.; Liang, Z.-Q.; Luo, M.; Wang, X.; Li, H.; O'Brien, C. P.; Tan, C.-S.; Nam, D.-H.; Quintero-Bermudez, R.; Zhuang, T.-T.; Li, Y. C.; Han, Z.; Britt, R. D.; Sinton, D.; Agapie, T.; Peters, J. C.; Sargent, E. H. Molecular Tuning of CO₂ -to-Ethylene Conversion. *Nature* **2020**, *577* (7791), 509–513. <https://doi.org/10.1038/s41586-019-1782-2>.
- (35) Thevenon, A.; Rosas-Hernández, A.; Fontani Herreros, A. M.; Agapie, T.; Peters, J. C. Dramatic HER Suppression on Ag Electrodes via Molecular Films for Highly Selective CO₂ to CO Reduction. *ACS Catal.* **2021**, *11* (8), 4530–4537. <https://doi.org/10.1021/acscatal.1c00338>.
- (36) Ren, D.; Fong, J.; Yeo, B. S. The Effects of Currents and Potentials on the Selectivities of Copper toward Carbon Dioxide Electroreduction. *Nat. Commun.* **2018**, *9* (1), 925. <https://doi.org/10.1038/s41467-018-03286-w>.
- (37) Hori, Y. Electrochemical CO₂ Reduction on Metal Electrodes. In *Modern Aspects of Electrochemistry*; Vayenas, C. G., White, R. E., Gamboa-Aldeco, M. E., Eds.; Springer: New York, 2008; Vol. 42, pp 89–189.
- (38) Kortlever, R.; Shen, J.; Schouten, K. J. P.; Calle-Vallejo, F.; Koper, M. T. M. Catalysts and Reaction Pathways for the Electrochemical Reduction of Carbon Dioxide. *J. Phys. Chem. Lett.* **2015**, *6* (20), 4073–4082. <https://doi.org/10.1021/acs.jpcllett.5b01559>.
- (39) Saberi Safaei, T.; Mephram, A.; Zheng, X.; Pang, Y.; Dinh, C.-T.; Liu, M.; Sinton, D.; Kelley, S. O.; Sargent, E. H. High-Density Nanosharp Microstructures Enable Efficient CO₂ Electroreduction. *Nano Lett.* **2016**, *16* (11), 7224–7228. <https://doi.org/10.1021/acs.nanolett.6b03615>.
- (40) Cheng, T.; Xiao, H.; Goddard, W. A. Full Atomistic Reaction Mechanism with Kinetics for CO Reduction on Cu(100) from Ab Initio Molecular Dynamics Free-Energy Calculations at 298 K. *Proc. Natl. Acad. Sci.* **2017**, *114* (8), 1795–1800. <https://doi.org/10.1073/pnas.1612106114>.
- (41) Garza, A. J.; Bell, A. T.; Head-Gordon, M. Mechanism of CO₂ Reduction at Copper Surfaces: Pathways to C₂ Products. *ACS Catal.* **2018**, *8* (2), 1490–1499. <https://doi.org/10.1021/acscatal.7b03477>.
- (42) Schreier, M.; Yoon, Y.; Jackson, M. N.; Surendranath, Y. Competition between H and CO for Active Sites Governs Copper-Mediated Electrosynthesis of Hydrocarbon Fuels. *Angew. Chem. Int. Ed.* **2018**, *57* (32), 10221–10225. <https://doi.org/10.1002/anie.201806051>.

- (43) Xiao, H.; Cheng, T.; Goddard, W. A. Atomistic Mechanisms Underlying Selectivities in C₁ and C₂ Products from Electrochemical Reduction of CO on Cu(111). *J. Am. Chem. Soc.* **2017**, *139* (1), 130–136. <https://doi.org/10.1021/jacs.6b06846>.
- (44) Other potential ways to disrupt the scaling relationship observed here include nanostructuring,^{14–17} higher overpotentials and current densities resulting in pH gradients,^{10–13,18} and bimetallic system engineering.^{19–21}